A Dynamic Knockout Reveals That Conformational Fluctuations Influence the Chemical Step of Enzyme Catalysis

Gira Bhabha *et al.*

Science **332**, 234 (2011);
DOI: 10.1126/science.1198542

Science (print ISSN 0036-8075; online ISSN 1095-9203) is published weekly, except the last week in December, by the American Association for the Advancement of Science, 1200 New York Avenue NW, Washington, DC 20005.

electron microscopy; E. Zaikova for qPCR assistance; and E. J. Pritham, J. Davies, and E. Nomis for constructive comments. Supported by the Natural Science and Engineering Research Council of Canada (NSERC) Discovery Grants Program, the Tula Foundation through the Centre for Microbial Diversity and Evolution, and fellowships awarded to M.G.F. by the Gottlieb Daimler- and Karl Benz-Foundation, Germany, and the University of British Columbia. The genome sequence of Mavirus has been deposited in GenBank under the accession number HQ712116.

Supporting Online Material
www.sciencemag.org/cgi/content/full/science.1199412/DC1
Materials and Methods
Figs. S1 to S8
Tables S1 to S3
References

22 October 2010; accepted 8 February 2011
Published online 3 March 2011;
10.1126/science.1199412

A Dynamic Knockout Reveals That Conformational Fluctuations Influence the Chemical Step of Enzyme Catalysis

Gira Bhabha,[1] Jeeyeon Lee,[2]* Damian C. Ekiert,[1] Jongsik Gam,[2] Ian A. Wilson,[1] H. Jane Dyson,[1] Stephen J. Benkovic,[2] Peter E. Wright[1]†

Conformational dynamics play a key role in enzyme catalysis. Although protein motions have clear implications for ligand flux, a role for dynamics in the chemical step of enzyme catalysis has not been clearly established. We generated a mutant of *Escherichia coli* dihydrofolate reductase that abrogates millisecond-time-scale fluctuations in the enzyme active site without perturbing its structural and electrostatic preorganization. This dynamic knockout severely impairs hydride transfer. Thus, we have found a link between conformational fluctuations on the millisecond time scale and the chemical step of an enzymatic reaction, with broad implications for our understanding of enzyme mechanisms and for design of novel protein catalysts.

Protein motions are critical for biological functions, but their precise role in enzyme catalysis remains unclear (*1*, *2*). Although there is convincing evidence that conformational fluctuations are essential for the mediation of substrate and cofactor binding as well as product release and can be rate-limiting for enzyme turnover (*3*–*6*), the importance of protein flexibility for progression along the chemical reaction coordinate remains a matter of debate (*7*, *8*). In one view, electrostatic preorganization of the active site is considered to account fully for enzyme catalysis (*9*); however, hydrogen tunneling experiments suggest that a static model is inadequate and that fluctuations that reorganize the active site are required for the chemical step (*7*, *10*, *11*), which involves conformational sampling to facilitate hydrogen transfer as well as the transfer itself.

Escherichia coli dihydrofolate reductase (*ec*DHFR) is a paradigm for understanding the relationship between structure, dynamics, and catalysis (*4*, *12*–*14*). DHFR catalyzes the stereospecific reduction of dihydrofolate (DHF) to tetrahydrofolate (THF) using reduced nicotinamide adenine dinucleotide phosphate (NADPH) as cofactor. Five intermediates have been identified in the steady-state catalytic cycle (*7*): E:NADPH, E:NADPH:DHF, E:NADP$^+$:THF, E:THF, and E:NADPH:THF (Fig. 1). Large conformational changes are observed in the Met20 loop (residues 9 to 24) between the Michaelis complex E:NADPH:DHF [modeled by E:NADP$^+$:folate (FOL) for structural studies] and the product complex, E:NADP$^+$:THF (*13*). The Met20 loop adopts two dominant conformations: the "closed" conformation, in which the loop packs tightly against the nicotinamide ring of the cofactor, and the "occluded" conformation, in which the loop projects into the active site and sterically blocks the nicotinamide-binding pocket. The holoenzyme (E:NADPH) and the model Michaelis complex (E:NADP$^+$:FOL) are in the closed conformation, whereas the three product complexes (E:NADP$^+$:THF, E:THF, and E:NADPH:THF) adopt the occluded conformation (Fig. 1), which is stabilized by hydrogen bonds between Asn23 and the backbone and side chain of Ser148 (*13*, *15*).

In crystal structures of human and other vertebrate DHFRs, the Met20 loop is invariably closed (*16*). Alignment of the human and *E. coli* DHFR protein sequences suggests that the occluded conformation is destabilized in the human enzyme because of an inability to form the stabilizing hydrogen bond made by the S148 side chain in *ec*DHFR (fig. S1). In addition, a

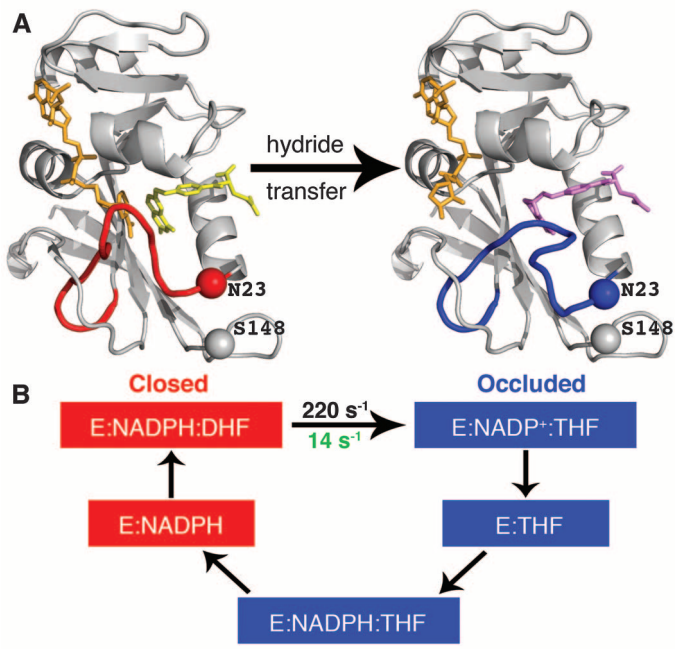

Fig. 1. Conformational changes that occur during the *E. coli* DHFR catalytic cycle. (**A**) (Left) Illustration of E:NADP$^+$:FOL crystal structure (1RX2, model for the Michaelis complex, E:NADPH:DHF) in the closed conformation. (Right) Crystal structure of E:NADP$^+$:ddTHF (1RX4, model for the product complex) in the occluded conformation. NADP$^+$ is shown in orange; FOL is shown in yellow, and ddTHF is shown in purple. Red indicates Met20 loop in the closed conformation; blue indicates Met20 loop in the occluded conformation. The sites of mutation, N23 and S148, are shown as spheres. (**B**) Intermediates in the wild-type *E. coli* DHFR catalytic cycle. Intermediates shown in red are in the closed conformation, and those in blue are in the occluded conformation. Before hydride transfer, the Met20 loop is in the closed conformation, in which it packs tightly against the nicotinamide ring of NADP$^+$. After hydride transfer, the Met20 loop adopts the occluded conformation, in which the nicotinamide ring of NADP$^+$ is sterically hindered from binding in the active site. NADP$^+$ undergoes a concurrent conformational change in which the nicotinamide ring is expelled from the binding pocket, initiating NADP$^+$ release from the ternary product complex. The rate of hydride transfer in the wild-type and N23PP/S148A mutant enzyme is indicated in black and green, respectively. The mutation alters the pathway used for product and NADP$^+$ release, as shown in fig. S2.

[1]Department of Molecular Biology and Skaggs Institute for Chemical Biology, The Scripps Research Institute, La Jolla, CA 92037, USA. [2]Department of Chemistry, Pennsylvania State University, University Park, PA 16802, USA.

*Present address: College of Pharmacy, Ajou University, San 5, Woncheon-dong, Yeongtong-Gu, Suwon 443-749, Korea.
†To whom correspondence should be addressed. E-mail: wright@scripps.edu

polyproline sequence (PWPP) at the end of the "Met20 loop" of human DHFR may render the loop less flexible than in the *E. coli* enzyme. We hypothesized that a "dynamic knockout" mutant designed to impair the dynamics of the Met20 loop in *ec*DHFR would give direct information on the role of active-site loop fluctuations in catalysis by the *E. coli* enzyme. To this end, the *ec*DHFR mutant N23PP/S148A (Fig. 1) was engineered and characterized by means of x-ray crystallography, nuclear magnetic resonance (NMR) spectroscopy, and kinetic analysis (*17*, *18*).

To assess the effect of the mutations on *ec*DHFR activity, we carried out both steady-state and pre-steady-state kinetic measurements on N23PP/S148A DHFR. The overall turnover rate (k_{cat}) is very much lower than for the wild-type enzyme (Table 1). For wild-type *ec*DHFR, k_{cat} is determined by dissociation of the THF product from the E:NADPH:THF complex (Fig. 1) (*10*), whereas for the mutant enzyme the magnitude of k_{cat} is determined by dissociation of the $NADP^+$ cofactor (fig. S2). Thus, the reduced flexibility inherent in the design of N23PP/S148A *ec*DHFR imposes a change in the kinetic step that determines the steady-state $k_{cat.}$ The hydride transfer step was monitored directly in pre-steady-state kinetic experiments, as described in (*17*) (fig. S3). The rate of hydride transfer at pH 7.0 is 14 s^{-1} for the N23PP/S148A DHFR mutant, which is significantly slower than for wild-type *ec*DHFR (Table 1) (*19*). The measured rate for the chemical step has a primary kinetic isotope effect (KIE) of 3.0 (the same as the wild-type enzyme), which is consistent with the difference in zero-point energies between the two hydrogen isotopes and confirms that we did indeed directly observe the rate of hydride transfer.

Table 1. Kinetic parameters. ND, not determined.

	Wild type*	N23PP-S148A	N23PP	S148A†
k_{cat} (s^{-1})	12	1.8 ± 0.6	2.5 ± 1	6.6 ± 0.8
k_{hyd} (s^{-1})	220 ± 10	13.9 ± 0.6	14.2 ± 1	157 ± 3
pK_a	6.5 ± 0.1	6.7 ± 0.1	6.6 ± 0.1	ND
KIE (k_{hyd})	3.0 ± 0.1	3.0 ± 0.1	ND	2.7 ± 0.1

*Kinetic parameters for wild-type enzyme, as reported in (*11*). †Kinetic parameters for the S148A mutant, as reported in (*26*).

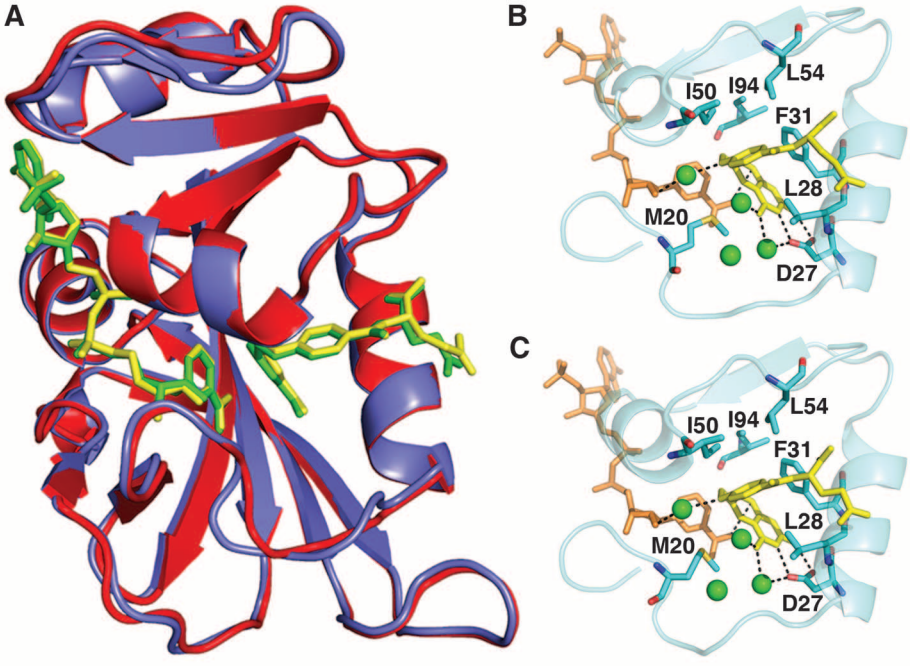

Fig. 2. The three-dimensional structures of the E:$NADP^+$:FOL complexes of the N23PP/S148A mutant and wild-type *E. coli* DHFR are almost identical. (**A**) Superposition of the crystal structures of wild-type *E. coli* DHFR (1RX2) and N23PP/S148A *E. coli* DHFR. Wild-type *E. coli* DHFR is shown in red with yellow ligands, and N23PP/S148A *E. coli* DHFR is shown in purple with green ligands. (**B**) Active-site configuration for wild-type ecDHFR (1RX2–re-refined). Folate is shown in yellow, $NADP^+$ is shown in orange, the waters are shown as green spheres, and key active-site residues are blue sticks. (**C**) Active-site configuration for N23PP/S148A ecDHFR. Colors are the same as for (B). For clarity, only the major conformation of the glutamate moiety of folate is shown. The active-site configurations are almost identical for wild-type and N23PP/S148A ecDHFR, including placement of polar residues, key hydrophobic residues, and waters, showing that the electrostatic nature of the active site is unchanged by the mutations.

Structural differences between N23PP/S148A *ec*DHFR and wild-type *ec*DHFR were assessed by determining the crystal structure of the mutant enzyme in complex with $NADP^+$ and folate and comparing it with the wild-type E:$NADP^+$:FOL complex (*13*). To eliminate differences in refinement methods, the wild-type E:$NADP^+$:FOL complex (*13*) was re-refined by using the structure factors deposited in the Protein Data Bank (PDB) (code:1RX2), as described in (*17*). The re-refined structure shows only very minor differences from the original 1RX2 coordinates. The N23PP/S148A *ec*DHFR at 1.6 Å resolution is almost identical to 1RX2–re-refined at 1.8 Å (Fig. 2) (*13*). Some minor adjustments at the end of the Met20 loop can be observed because of the proline insertion, but the loop is clearly in the closed conformation as in the wild-type E:$NADP^+$:FOL complex. The ligand (fig. S4) and active-site side-chain conformations are maintained (Fig. 2), as are the hydrogen bonds (table S2) and the locations of water molecules in the active site. The distance between hydride donor and acceptor atoms is slightly decreased (from 3.3 to 2.9 Å) in the N23PP/S148A mutant. This decrease cannot account for the impaired hydride transfer rate in the mutant because a shorter distance would be expected to facilitate hydride transfer, not inhibit it. The similarity of the backbone conformations of the wild-type and N23PP/S148A E:$NADP^+$:FOL complexes in solution is also illustrated by the similarity of ^{15}N and ^1H chemical shifts (fig. S5).

The conservation of side-chain conformations and water molecules in the active site of the wild-type and mutant enzymes argues for a very similar electrostatic environment. However, a slight change in the Met20 side chain required further investigation. It has been proposed that the Met20 S_δ atom might assist catalysis by increasing the pK_a of the substrate (where K_a is the acid dissociation constant), promoting protonation of the N5 atom of the pterin (*20*). The Met20 S_δ atom in N23PP/S148A E:$NADP^+$:FOL is shifted ~0.3 Å relative to its position in the wild-type complex (fig. S6) (*21*). We measured the pH-dependence of hydride transfer in the N23PP/S148A mutant to ensure that the apparent small difference in the position of the Met20 S_δ atom does not impair hydride transfer by decreasing the pK_a for N5. The hydride transfer rate for N23PP/S148A ecDHFR decreases with increasing pH (*22*) with a pK_a of 6.7 ± 0.1, which is the same, within experimental error, as the value for the wild-type enzyme (6.5 ± 0.1). If anything, the pK_a is slightly higher for the mutant enzyme, which would facilitate hydride transfer rather than inhibit it. Thus, the x-ray and NMR data and the pK_a measurements show that there are no substantial differences in the structure or electrostatic environment

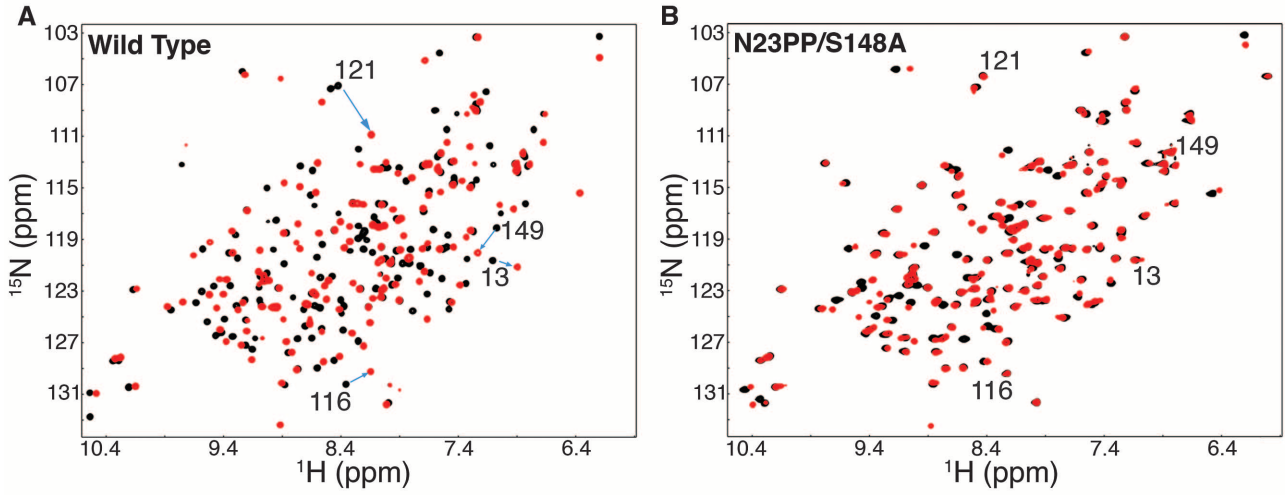

Fig. 3. The Met20 loop of N23PP/S148A *E. coli* DHFR remains in the closed position across the chemical step. (**A**) ^{1}H-^{15}N HSQC spectra of wild-type E:NADP^{+}:FOL (model Michaelis complex, black) in the closed conformation and E:NADP^{+}:THF (product complex, red) in the occluded conformation. Large chemical shift differences are observed, particularly for residues in regions that undergo the closed-to-occluded structural change. Chemical shift changes from closed (black) to occluded (red) are indicated by arrows for several residues in the active-site loops. (**B**) ^{1}H-^{15}N HSQC spectra of N23PP/S148A E:NADP^{+}:FOL (model Michaelis complex, black) and E:NADP^{+}:THF (product complex, red). The ^{1}H-^{15}N HSQC spectra for the complexes of the mutant enzyme are similar; the cross peaks corresponding to the active-site loops do not shift and appear in the position corresponding to the closed conformation for both complexes. A quantitative chemical shift analysis is presented in fig. S8.

of the active site between the E:NADP^{+}:FOL complexes of wild-type and N23PP/S148A ecDHFR.

In wild-type ecDHFR, the Met20 loop adopts the closed ground-state conformation in the Michaelis model complex, E:NADP^{+}:FOL, and the occluded ground-state conformation in the product ternary complex, E:NADP^{+}:THF (*13*, *15*, *23*). Previous NMR studies identified marker resonances, mostly in the Met20 and FG loops, for which ^{15}N and ^{1}H chemical shifts differ markedly between the closed and occluded conformations (*23*). Unlike the wild-type enzyme, the E:NADP^{+}:FOL and E:NADP^{+}:THF complexes of the N23PP/S148A mutant enzyme have almost identical ^{1}H and ^{15}N chemical shifts for most residues, including those in the Met20, FG, and GH loops (Fig. 3 and fig. S7), showing that the mutant enzyme remains in the closed conformation across the chemical step. The occluded conformation itself is not relevant to hydride transfer, which takes place within an ensemble of states in which the active site loops are closed (*13*). However, the fact that the mutant enzyme is unable to adopt an occluded conformation suggested that the flexibility of the active site loops may be considerably dampened and prompted us to examine the dynamics of the N23PP/S148A Michaelis model complex (E:NADP^{+}:FOL).

Carr-Purcell-Meiboom-Gill (CPMG)–based ^{15}N R_2 relaxation dispersion NMR experiments were used to monitor the sampling of higher-energy, lowly populated conformational substates that are associated with millisecond-time-scale structural fluctuations (*24*, *25*). Previous studies of wild-type *ec*DHFR revealed millisecond-time-scale motions in the active site and C-terminal region in all five intermediate complexes of the catalytic cycle (*4*, *26*). Surprisingly, relaxation dispersion experiments on the E:NADP^{+}:FOL complex of N23PP/S148A DHFR showed no dispersion for any active site residues (with the sole exception of Ala9), indicating that fluctuations on the millisecond time scale are abrogated in the mutant enzyme complex (Fig. 4). Residues associated with the C terminus, however, undergo fluctuations on the millisecond time scale similar to those in the wild-type enzyme, confirming that the mutations affect dynamics only in the active site. R_1, R_2, and heteronuclear nuclear Overhauser effect (NOE) experiments show that the Met20 loop of N23PP/S148A in the E:NADP^{+}:FOL complex is rather rigid on the picosecond to nanosecond time scale, as in the wild-type enzyme (fig. S8) (*27*). Several residues exhibiting exchange contributions from millisecond-time-scale conformational fluctuations in the active-site loops have elevated R_2 values in wild-type *ec*DHFR, whereas the values for these residues remain close to average for the N23PP/S148A mutant, suggesting that the mutations have not simply shifted the motions to a faster, microsecond time scale. No minor resonances, which might be expected if there was a small population (~3% or higher) of an alternative loop conformation in slow exchange with the closed ground state, were observed in the ^{15}N-HSQC spectrum of N23PP/S148A E:NADP^{+}:FOL. Thus, we conclude that the millisecond-time-scale fluctuations in the active site of the wild-type enzyme have been abolished in the N23PP/S148A mutant.

To obtain further insights into the effects of the N23PP/S148A mutations, we generated two additional *ec*DHFR mutants, N23PP and S148A. The N23PP mutation is in itself sufficient to abrogate the active-site flexibility required for efficient catalysis. The hydride transfer rate for the N23PP mutant (14 ± 1 s^{-1}) is the same as for N23PP/S148A. NMR experiments show that the Met20 loop remains in the closed conformation across the hydride transfer step and that the millisecond-time-scale fluctuations in the active site are quenched in the E:NADP^{+}:FOL complex of N23PP DHFR (Fig. 4, Table 1, and fig. S9). An analysis of S148A *ec*DHFR reveals that the decreased hydride transfer rate does not simply arise from impairment of the closed-to-occluded transition in the mutant enzymes. S148A *ec*DHFR also remains in the closed ground-state conformation across the hydride transfer step (fig. S10), yet its hydride transfer rate (157 s^{-1}) is decreased only slightly from that of the wild-type enzyme (*28*). R_2 dispersion experiments on the S148A E:NADP^{+}:FOL complex show that although the millisecond-time-scale dynamics are dampened as compared with wild type, several active-site residues do retain flexibility, sampling higher-energy conformational substates that do not correspond to the occluded state (Fig. 4 and fig. S11). We conclude that unlike the N23PP and N23PP/S148A mutants, the S148A mutant retains residual motions in the active site, which are not associated with the closed-occluded transition but which probably play a role in promoting hydride transfer.

Considering that the E:NADP^{+}:FOL complexes, which are models for the Michaelis complex, have virtually identical active-site structures in both the N23PP/S148A mutant and wild-type enzyme, it is most unlikely that hydride transfer is impaired in the mutant because of differences in the structural and electrostatic environment of the active site. Although the ground-state structures are almost indistinguishable, the wild-type and mutant enzymes differ substantially in their ability to sample alternative ground-state active-site confor-

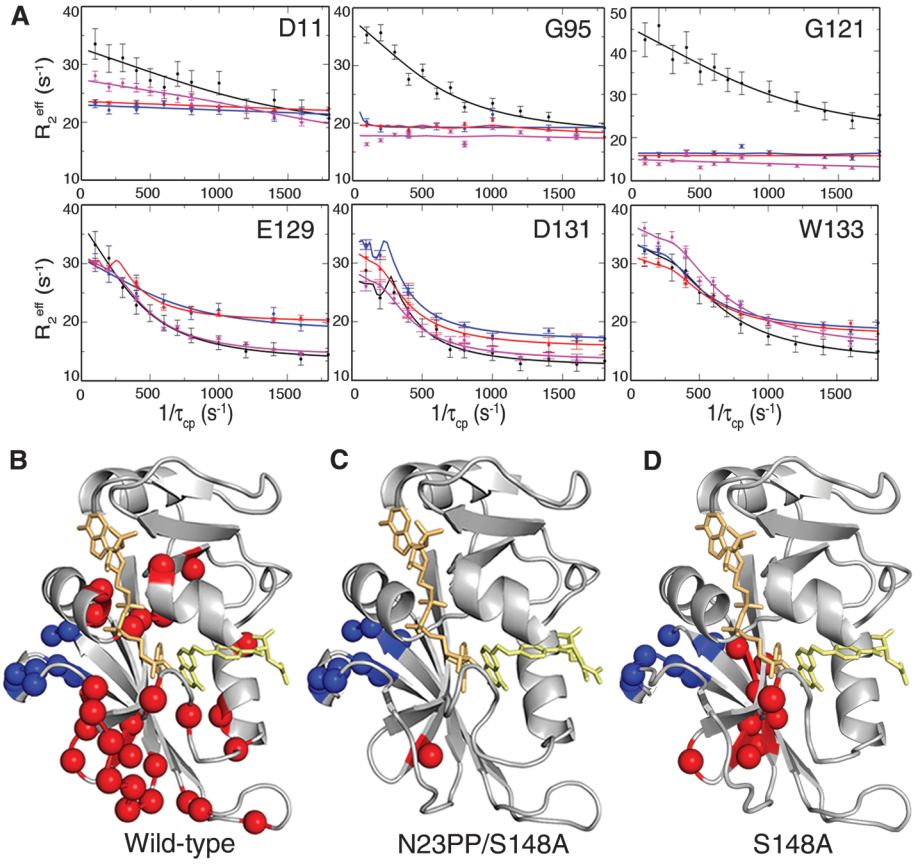

Fig. 4. Millisecond-time-scale dynamics in the active-site loops of the E:NADP$^+$:FOL complex are impaired by the N23PP/S148A mutation. (**A**) Representative ^{15}N R_2 relaxation dispersion curves for (black) wild-type, (red) N23PP/S148A, (blue) N23PP, and (purple) S148A E:NADP$^+$:FOL. Dispersion data were collected at pH 7.6 and at 301 K. (Top) Active-site loop residues (11, 95, and 121), for which the dispersion observed in wild-type E:NADP$^+$:FOL is not observed in either N23PP/S148A or N23PP E:NADP$^+$:FOL. S148A retains dispersion for residue 11 and other active-site residues, as shown in fig. S11. (Bottom) C-terminal–associated residues (129, 131, and 133), for which dispersion is observed for the wild-type and mutant proteins. Residues that display ^{15}N relaxation dispersion in the E:NADP$^+$:FOL complex are mapped onto the structure for (**B**) wild type, (**C**) N23PP/S148A, and (**D**) S148A. 1RX2 coordinates are used for representations in (B) and (D). Red spheres indicate active-site–associated residues for which R_2 dispersion is observed. Blue spheres indicate C-terminal–associated residues for which R_2 dispersion is observed. NADP$^+$ is shown as orange sticks, and FOL is shown as yellow sticks. For clarity, only the major conformation of the glutamate moiety of folate is shown.

mations and access higher-energy conformational substates through millisecond-time-scale fluctuations. The ground-state conformational change between the closed Michaelis complex and the occluded product complex in wild-type *ec*DHFR is not observed for any of the three mutants because the active-site loops are restrained in the closed conformation. The millisecond-time-scale motions in the active site that allow the wild-type enzyme to sample higher-energy substates are eliminated in the N23PP/S148A and N32PP mutants, whereas the S148A mutant still retains some flexibility and has a correspondingly higher rate of hydride transfer. We therefore conclude that the greatly decreased rate of hydride transfer in the N23PP/S148A and N32PP mutant enzymes does not result from changes in structural or electrostatic preorganization of the active site but from impaired flexibility.

Molecular simulations consistently show that Met20 loop residues move closer to the cofactor on progressing from reactant to transition state. These residues are predicted to play an important role in electrostatic stabilization of the transition state and in promoting protonation of the N5 atom of the pterin moiety of the substrate (*20*, *29*, *30*). This movement is probably required to tightly close and compact the active site, to correctly orient and constrain the substrate and cofactor, and to promote hydride transfer by reducing the distance between the donor and acceptor atoms. Although the active site of the N23PP/S148A *ec*DHFR mutant is fully preorganized in the ground state, millisecond-time-scale fluctuations of the active site are restricted so that the enzyme cannot efficiently sample higher-energy conformational substates that are conducive to formation of the transition state; impairment of conformational fluctuations in the active site leads to strong inhibition of the chemical step. Fine-tuning of conformational flexibility is probably a general phenomenon that can be harnessed in the engineering of efficient protein catalysts.

References and Notes

1. S. Hammes-Schiffer, S. J. Benkovic, *Annu. Rev. Biochem.* **75**, 519 (2006).
2. K. Henzler-Wildman, D. Kern, *Nature* **450**, 964 (2007).
3. M. Wolf-Watz *et al.*, *Nat. Struct. Mol. Biol.* **11**, 945 (2004).
4. D. D. Boehr, D. McElheny, H. J. Dyson, P. E. Wright, *Science* **313**, 1638 (2006).
5. N. Doucet, E. D. Watt, J. P. Loria, *Biochemistry* **48**, 7160 (2009).
6. E. D. Watt, H. Shimada, E. L. Kovrigin, J. P. Loria, *Proc. Natl. Acad. Sci. U.S.A.* **104**, 11981 (2007).
7. Z. D. Nagel, J. P. Klinman, *Nat. Chem. Biol.* **5**, 543 (2009).
8. S. C. Kamerlin, A. Warshel, *Proteins* **78**, 1339 (2010).
9. A. V. Pisliakov, J. Cao, S. C. Kamerlin, A. Warshel, *Proc. Natl. Acad. Sci. U.S.A.* **106**, 17359 (2009).
10. Z. X. Liang, T. Lee, K. A. Resing, N. G. Ahn, J. P. Klinman, *Proc. Natl. Acad. Sci. U.S.A.* **101**, 9556 (2004).
11. S. J. Benkovic, S. Hammes-Schiffer, *Science* **301**, 1196 (2003).
12. C. A. Fierke, K. A. Johnson, S. J. Benkovic, *Biochemistry* **26**, 4085 (1987).
13. M. R. Sawaya, J. Kraut, *Biochemistry* **36**, 586 (1997).
14. J. R. Schnell, H. J. Dyson, P. E. Wright, *Annu. Rev. Biophys. Biomol. Struct.* **33**, 119 (2004).
15. R. P. Venkitakrishnan *et al.*, *Biochemistry* **43**, 16046 (2004).
16. J. F. Davies 2nd *et al.*, *Biochemistry* **29**, 9467 (1990).
17. Materials and methods are available as supporting material on *Science* Online.
18. Single-letter abbreviations for the amino acid residues are as follows: A, Ala; C, Cys; D, Asp; E, Glu; F, Phe; G, Gly; H, His; I, Ile; K, Lys; L, Leu; M, Met; N, Asn; P, Pro; Q, Gln; R, Arg; S, Ser; T, Thr; V, Val; W, Trp; and Y, Tyr. In the mutants, other amino acids were substituted at certain locations; for example, H134R indicates that histidine at position 134 was replaced by arginine.
19. C. E. Cameron, S. J. Benkovic, *Biochemistry* **36**, 15792 (1997).
20. I. V. Khavrutskii, D. J. Price, J. Lee, C. L. Brooks 3rd, *Protein Sci.* **16**, 1087 (2007).
21. The terminal methyl of M20 is not clearly defined by the electron density in 1RX2 and in 1RX2–re-refined, and is probably flexible. In addition, density for water 47 is observed in 1RX2–re-refined but was not built into 1RX2. A discussion on building M20 and water47 into 1RX2-rerefined is included in the supporting online material (SOM) text.
22. At basic pHs, the hydride transfer rate (k_{hyd}) is decreased to 3.3 s^{-1} for N23PP/S148A because of the limited sources of protons for the hydride transfer step. The pK_a values are derived from fitting the pH versus k_{hyd} profile as described in (*17*).
23. M. J. Osborne, R. P. Venkitakrishnan, H. J. Dyson, P. E. Wright, *Protein Sci.* **12**, 2230 (2003).
24. A. G. Palmer 3rd, C. D. Kroenke, J. P. Loria, *Methods Enzymol.* **339**, 204 (2001).
25. A. Mittermaier, L. E. Kay, *Science* **312**, 224 (2006).
26. D. McElheny, J. R. Schnell, J. C. Lansing, H. J. Dyson, P. E. Wright, *Proc. Natl. Acad. Sci. U.S.A.* **102**, 5032 (2005).
27. M. J. Osborne, J. Schnell, S. J. Benkovic, H. J. Dyson, P. E. Wright, *Biochemistry* **40**, 9846 (2001).
28. G. P. Miller, D. C. Wahnon, S. J. Benkovic, *Biochemistry* **40**, 867 (2001).
29. P. K. Agarwal, S. R. Billeter, P. T. Rajagopalan, S. J. Benkovic, S. Hammes-Schiffer, *Proc. Natl. Acad. Sci. U.S.A.* **99**, 2794 (2002).
30. M. Garcia-Viloca, D. G. Truhlar, J. Gao, *Biochemistry* **42**, 13558 (2003).

31. The authors acknowledge L. Tuttle for invaluable discussions, S. Bae for NMR data on the S148A mutant, H. Tien and D. Marciano of the Robotics Core at the Joint Center for Structural Genomics (JCSG) for automated crystal screening, and X. Dai for technical assistance with crystallographic data collection. This work was supported by the National Institutes of Health (NIH) grant GM75995 and the Skaggs Institute of Chemical Biology. The JCSG is supported by NIH National Institute of General Medical Sciences (NIGMS) (U54 GM094586). D.C.E. is supported by a predoctoral fellowship from the Achievement Rewards for College Scientists Foundation and grant GM080209 from the NIH Molecular Evolution Training Program. The GM/CA CAT 23-ID-D has been funded in whole or in part with federal funds from National Cancer Institute (Y1-CO-1020) and NIGMS (Y1-GM-1104). Use of the Advanced Photon Source (APS) was supported by the U.S. Department of Energy, Basic Energy Sciences, Office of Science, under contract DE-AC02-06CH11357. The content is solely the responsibility of the authors and does not necessarily represent the official views of NIGMS or NIH. Coordinates and structure factors of N23PP/S148A ecDHFR and 1RX2–re-refined are deposited in PDB (code 3QL0 and 3QL3). G.B. and P.E.W. designed the research. G.B. performed NMR experiments. G.B. and D.C.E. performed crystallography experiments and structure refinement. I.A.W. supervised structure refinement. J.L. and J.G. performed kinetic experiments and analysis. G.B., P.E.W., and S.J.B. analyzed and interpreted the data. G.B., P.E.W., and J.L. wrote the manuscript. I.A.W., H.J.D., and S.J.B. edited the manuscript.

Supporting Online Material

www.sciencemag.org/cgi/content/full/332/6026/234/DC1
Materials and Methods
SOM Text
Figs. S1 to S11
Tables S1 to S3
References

1 October 2010; accepted 16 February 2011
10.1126/science.1198542

Mutations in U4atac snRNA, a Component of the Minor Spliceosome, in the Developmental Disorder MOPD I

Huiling He,[1,2] Sandya Liyanarachchi,[1,2]* Keiko Akagi,[1,2]* Rebecca Nagy,[1,3]* Jingfeng Li,[1,2]* Rosemary C. Dietrich,[4] Wei Li,[1,2] Nikhil Sebastian,[1,2] Bernard Wen,[1,2] Baozhong Xin,[5] Jarnail Singh,[4] Pearlly Yan,[1,2] Hansjuerg Alder,[1,2] Eric Haan,[6,7] Dagmar Wieczorek,[8] Beate Albrecht,[8] Erik Puffenberger,[9] Heng Wang,[5] Judith A. Westman,[1,3] Richard A. Padgett,[4] David E. Symer,[1,2,3,10] Albert de la Chapelle[1,2]†

Small nuclear RNAs (snRNAs) are essential factors in messenger RNA splicing. By means of homozygosity mapping and deep sequencing, we show that a gene encoding U4atac snRNA, a component of the minor U12-dependent spliceosome, is mutated in individuals with microcephalic osteodysplastic primordial dwarfism type I (MOPD I), a severe developmental disorder characterized by extreme intrauterine growth retardation and multiple organ abnormalities. Functional assays showed that mutations (30G>A, 51G>A, 55G>A, and 111G>A) associated with MOPD I cause defective U12-dependent splicing. Endogenous U12-dependent but not U2-dependent introns were found to be poorly spliced in MOPD I patient fibroblast cells. The introduction of wild-type U4atac snRNA into MOPD I cells enhanced U12-dependent splicing. These results illustrate the critical role of minor intron splicing in human development.

The small nuclear RNA (snRNA) U4atac is a component of the minor spliceosome and is required for the proper excision of the U12-dependent class of introns (*1*–*4*). Although they account for only about 800 introns in humans, U12-dependent introns are found in many essential genes, such as those involved in DNA replication and repair, transcription, and RNA processing and translation (*5*). Thus, mutations in an snRNA required to splice such introns are likely deleterious and presumably would result in important developmental or clinical consequences.

U4atac snRNA appears to be encoded by a single gene (*RNU4ATAC*) on chromosome 2q14.2. Here we report that biallelic mutations in this gene are found in a severe developmental disorder, microcephalic osteodysplastic primordial dwarfism type I (MOPD I; also known as Taybi-Linder syndrome, OMIM 210710) (*6*). The main features of MOPD I patients are extreme intrauterine growth retardation, abnormalities in multiple organs, and death in infancy or early childhood (*7*, *8*). We focused our initial studies on cases diagnosed in the Amish of Ohio (*9*) (fig. S1), where uniform phenotypic features and a high degree of consanguinity suggested the existence of a single founder mutation. Briefly, we applied genome-wide homozygosity mapping followed by targeted, high-throughput second-generation sequencing in search of mutations at chromosome 2q14.2 (Fig. 1 and figs. S2 to S4). A novel g.51G>A variant within the non–protein-coding *RNU4ATAC* gene was detected in homozygosity in all seven Amish patients studied and in heterozygosity in 13 Amish parents. An Australian patient had the same mutation, whereas in two German MOPD 1 families, biallelic g.55G>A occurred in one patient and compound heterozygous g.30G>A and g.111G>A occurred in another patient. The 51G>A mutation represents a founder event in the Amish, as shown by haplotype analysis (figs. S3 and S5). This mutation was found in 16 of 281 Ohio Amish controls but in none of 180 Pennsylvania Amish controls. It was also seen in two of 720 controls from central Ohio but in none of 370 controls from France. The three mutations found in German MOPD 1 families were not found in 452 central Ohio controls. We conclude that the genetic findings are fully compatible with the expected recessive inheritance of rare mutations in the same gene [see (*9*) for further details of the mapping, sequencing, mutation analyses, and haplotyping].

The 30G>A, 51G>A, and 55G>A mutations in the U4atac snRNA are located within an important structural feature known as the 5′ stem-loop; the 111G>A mutation is located in another essential stem region, the 3′ stem-loop (*10*). These mutations are predicted to disrupt the snRNA's secondary structure and cause defects in the minor spliceosome (fig. S6) (*11*–*13*). To evaluate the functional effects of these mutations, we assayed the in vivo splicing of a modified U12-dependent intron reporter whose splicing is dependent on expression of a modified, exogenous U4atac snRNA, denoted U4atac-ATH (figs. S7 and S8) (*10*). Relative to wild-type U4atac, each of the MOPD I mutations in U4atac snRNA reduced U12-dependent splicing activity by greater than 90% (Fig. 2A). This suggests that all four mutations cause severe defects in U12-dependent splicing. Most of the splicing defect of the 51G>A mutation could be rescued by combining it with the 32C>T mutation in the presumed base-pairing partner (Fig. 2A, lane 8, and fig. S6). This suggests that the MOPD I mutation abrogates U4atac snRNA function by disrupting the RNA secondary structure.

U12-dependent introns are conserved in a variety of gene families implicated in different physiological processes (*5*, *14*). To assess U12-dependent splicing in MOPD I cells, we compared fibroblasts obtained from two MOPD I patients (with the 51G>A mutation) and two normal human fibroblast cell lines. Using real-time reverse transcription polymerase chain re-

[1]Human Cancer Genetics Program, Ohio State University, Columbus, OH 43210, USA. [2]Department of Molecular Virology, Immunology and Medical Genetics, School of Biomedical Science, Ohio State University, Columbus, OH 43210, USA. [3]Department of Internal Medicine, Ohio State University Comprehensive Cancer Center, Columbus, OH 43210, USA. [4]Department of Molecular Genetics, Lerner Research Institute, Cleveland Clinic, Cleveland, OH 44195, USA. [5]DDC Clinic for Special Needs Children, Middlefield, OH 44062, USA. [6]South Australian Clinical Genetics Service, SA Pathology (at Women's and Children's Hospital), North Adelaide, SA 5006, Australia. [7]Department of Pediatrics, University of Adelaide, Adelaide, SA 5005, Australia. [8]Institut für Humangenetik, Universitätsklinikum, Essen, Germany. [9]The Clinic for Special Children, Strasburg, PA 17579, USA. [10]Department of Biomedical Informatics, Ohio State University, Columbus, OH 43210, USA.

*These authors contributed equally to this work.
†To whom correspondence should be addressed. E-mail: albert.delachapelle@osumc.edu